



Design, synthesis and biological evaluation of anilide (dicarboxylic acid) shikonin esters as antitumor agents through targeting PI3K/Akt/mTOR signaling pathway

Yingying Ma^{a,1}, Xiaorong Yang^{b,1}, Hongwei Han^{a,c,1}, Zhongling Wen^a, Minkai Yang^a, Yahan Zhang^a, Jiangyan Fu^a, Xuan Wang^a, Tongming Yin^c, Guihua Lu^{a,c}, Jinliang Qi^{a,c}, Hongyan Lin^{a,c,*}, Xiaoming Wang^{a,c,*}, Yonghua Yang^{a,c,*}

^a State Key Laboratory of Pharmaceutical Biotechnology, Institute of Plant Molecular Biology, School of Life Sciences, Nanjing University, Nanjing 210023, China

^b School of Biology and Geography Science, Yili Normal University, Yining 835000, China

^c Co-Innovation Center for Sustainable Forestry in Southern China, Nanjing Forestry University, Nanjing 210037, China

ARTICLE INFO

Keywords:

TNBC
PI3K/Akt/mTOR
Anilide (dicarboxylic acid) shikonin esters
Antitumor
3D-QSAR

ABSTRACT

Triple-negative breast cancer (TNBC) has an unfavorable prognosis attribute to its low differentiation, rapid proliferation and high distant metastasis rate. PI3K/Akt/mTOR as an intracellular signaling pathway plays a key role in the cell proliferation, migration, invasion, metabolism and regeneration. In this work, we designed and synthesized a series of anilide (dicarboxylic acid) shikonin esters targeting PI3K/Akt/mTOR signaling pathway, and assessed their antitumor effects. Through three rounds of screening by computer-aided drug design method (CADD), we preliminarily obtained sixteen novel anilide (dicarboxylic acid) shikonin esters and identified them as excellent compounds. CCK-8 assay results demonstrated that compound M9 exhibited better antiproliferative activities against MDA-MB-231, A549 and HeLa cell lines than shikonin (SK), especially for MDA-MB-231 (M9: $IC_{50} = 4.52 \pm 0.28 \mu\text{M}$; SK: $IC_{50} = 7.62 \pm 0.26 \mu\text{M}$). Moreover, the antiproliferative activity of M9 was better than that of paclitaxel. Further pharmacological studies showed that M9 could induce apoptosis of MDA-MB-231 cells and arrest the cell cycle in G2/M phase. M9 also inhibited the migration of MDA-MB-231 cells by inhibiting Wnt/ β -catenin signaling pathway. In addition, western blot results showed that M9 could inhibit cell proliferation and migration by down-regulating PI3K/Akt/mTOR signaling pathway. Finally, a three-dimensional quantitative structure–activity relationship (3D-QSAR) model was also constructed to provide a basis for further development of shikonin derivatives as potential antitumor drugs through structure–activity relationship analysis. To sum up, M9 could be a potential candidate for TNBC therapy.

1. Introduction

Breast cancer is a common malignant tumor in women across the world. A recent epidemiological clinical study reported that the prevalence of breast cancer is over 10% [1,2]. Triple-negative breast cancer (TNBC) is a subtype of breast cancer characterized by negative expression of estrogen receptor (ER), progesterone receptor (PR) and human epidermal growth factor receptor 2 (HER2 or EGFR). More threateningly, about 30%-40% of TNBC can develop into metastatic breast cancer. Amongst, visceral metastasis is widespread, especially in the lung and brain [3,4]. Currently, the main clinical drugs for TNBC are

paclitaxel and Olaparib. Although there are various chemotherapy regimens, 35% of TNBC patients still have recurrence and metastasis [5]. There are some targeted drugs for TNBC in preclinical research and clinical trials, but most of them have not achieved the desired effect and have no apparent improvement in patients' Overall survival. This could be correlated with different subtypes of TNBC and the high heterogeneity of tumor cell signaling pathways, which suggests that we need to explore more potential targets for TNBC. Therefore, it is still a significant challenge for humans to discover more effective TNBC therapy.

Numerous studies indicate that the PI3K/Akt/mTOR signaling pathway is abnormally activated in patients with TNBC [6]. It is

* Corresponding authors at: State Key Laboratory of Pharmaceutical Biotechnology, Nanjing University, Nanjing 210023, China (Y. Yang, X. Wang, H. Lin).

E-mail addresses: linhy@nju.edu.cn (H. Lin), wangxm07@nju.edu.cn (X. Wang), yangyh@nju.edu.cn (Y. Yang).

¹ These authors contributed equally to this work.

commonly present in cells and is involved in the complex regulation of cell senescence, angiogenesis, energy metabolism and glucose metabolism, and is closely related to many other signaling pathways. Over-activation of this pathway can promote cell proliferation and abnormal differentiation, thereby mediating the generation, metastasis and invasion of tumors. Thus, it is crucial for the occurrence, development and prognosis of tumors. In this pathway, Akt is a core member of PI3K/Akt/mTOR signaling pathway, and its' over-activation can lead to tumorigenesis, metastasis and the generation of drug resistance [7].

Shikonin and its derivatives commonly possess antibacterial, anti-tumor, antiviral, anti-inflammatory and other pharmacological effects [8–12]. Previous studies indicate that shikonin and its derivatives can induce apoptosis in various cancer cell lines through inhibiting the PI3K/Akt/mTOR pathway [13–18]. In addition, some other studies have shown that shikonin derivatives such as SYUNZ-16 [19] and DMAKO-05 [20] can inhibit Akt activity and induce apoptosis, thereby inhibiting the occurrence and development of tumor. In this study, we first used a computer-aided drug design (CADD) approach to screen out 16 potential candidates for targeting the PI3K/Akt/mTOR signaling pathway. Based on the CADD results, we performed further biochemical and pharmaceutical analysis to evaluate the 16 novel anilide (dicarboxylic acid) shikonin esters as potent antitumor agents for TNBC through regulating PI3K/Akt/mTOR signaling pathway. Finally, we use 3D-QSAR software (discovery studio 3.5, Accelrys, Co. Ltd) to provides reference for the structural optimization of shikonin derivatives that inhibit the proliferation of MDA-MB-231 cells in the subsequent experiments.

2. Results and discussion

2.1. Preliminary calculation

Before synthesis, CADD method was used for three rounds of structural screening. Molecular docking was performed to calculate the binding energy (CDOCKERINTERACTION ENERGY in CDOCKER protocol in Discovery Studio 3.5) between all target compounds and Akt (PDB code: 3CQW) complex structure. In the first round, 33 compounds were evaluated to screen out the backbone. Then, the length of the intermediate bridge of shikonin derivatives was changed in the first round of screening to carry out the second round of screening. Next, the substituents on the benzene ring were changed to provide 15 options for the third round of screening. Totally, >2000 compounds were recalculated during the process of virtual screening and 16 compounds were selected for further study. (Supporting Information).

In terms of the binding energy, M9 (−49.0427 kcal/mol) was the best one amongst the 16 target compounds and its binding energy was much lower than SK (−28.163 kcal/mol) (Fig. S1, Supporting Information). In order to better understand the potential of M9, we listed all the amino acid residues that M9 interacted with Akt (PDB code: 3CQW), and the results were shown in Fig. 1. In this binding model, M9 can stably bind to the active cavity of Akt by forming the hydrogen bond with GLU278. Other weak interactions, such as Pi-Anion force, carbon-hydrogen bond, van der Waals and Pi-alkyl interactions which were formed with HIS354, GLU314, LFU347, PRO313, LYS276, TYR315, LEU277,

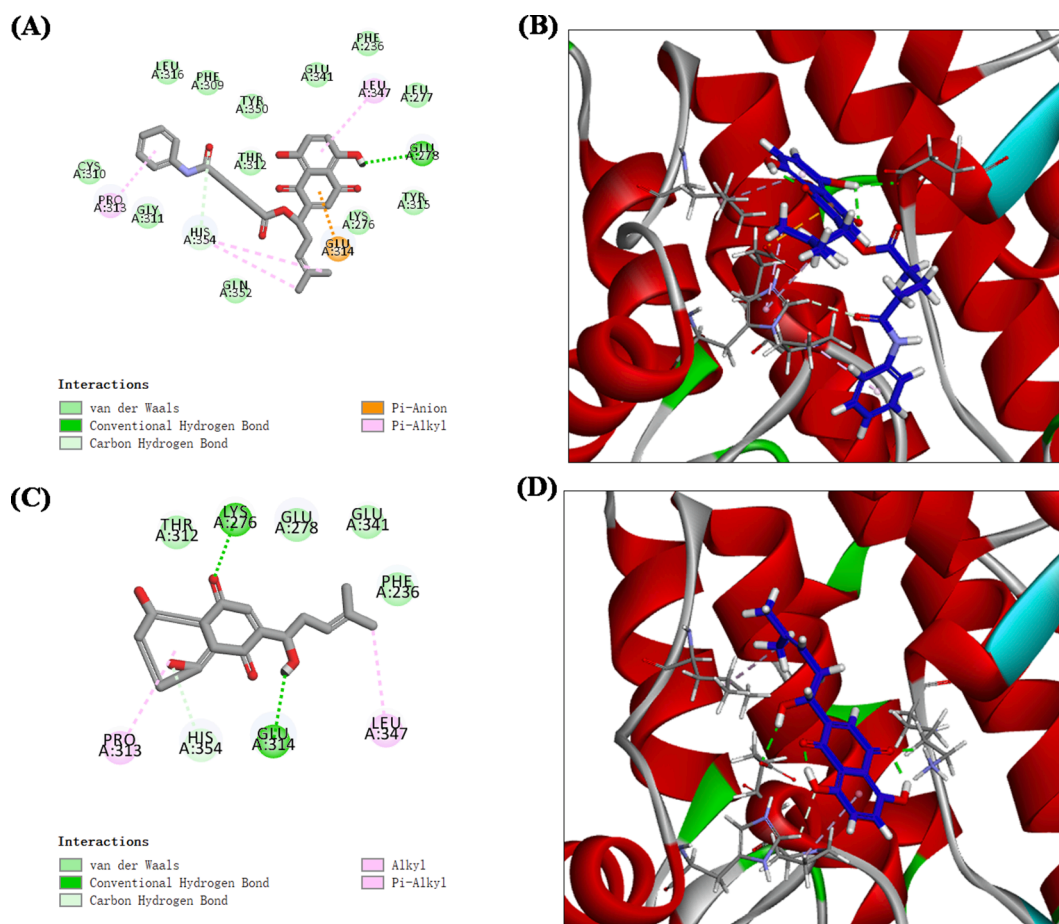


Fig. 1. The binding mode analysis of M9 and SK (PDB Code: 3CQW). (PDB code: 3CQW). (A) Two-dimensional image of M9 interacting with amino acid residues in the active cavity of Akt. (B) Three-dimensional image of M9 inserted into the Akt binding site. (C) Two-dimensional image of SK interacting with amino acid residues in the active cavity of Akt. (D) Three-dimensional image of SK inserted into the Akt binding site. Carbon atoms are color gray (2D image) or blue (3D image), oxygen atoms are color red, hydrogen atoms are color white. (For interpretation of the references to color in this figure legend, the reader is referred to the web version of this article.)

PHF236, GLU341 etc. In comparison, SK (the positive control) formed two hydrogen bonds with the amino acid residues (LYS276 and GLU314) of Akt, but the binding remained unstable because its structure is too small to match the active cavity.

2.2. Chemistry

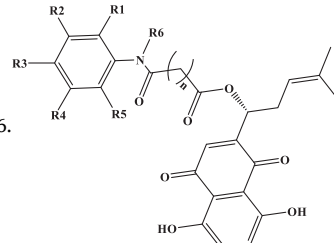
Synthesis routes of the anilide (dicarboxylic acid) shikonin esters M1-M16 were shown in Scheme 1. All of the target compounds were reported for the first time here, and their structures were fully characterized by HRMS, ^1H NMR, ^{13}C NMR and melting test. The results were completely consistent with the structure described. (Supporting Information).

2.3. Biological activities

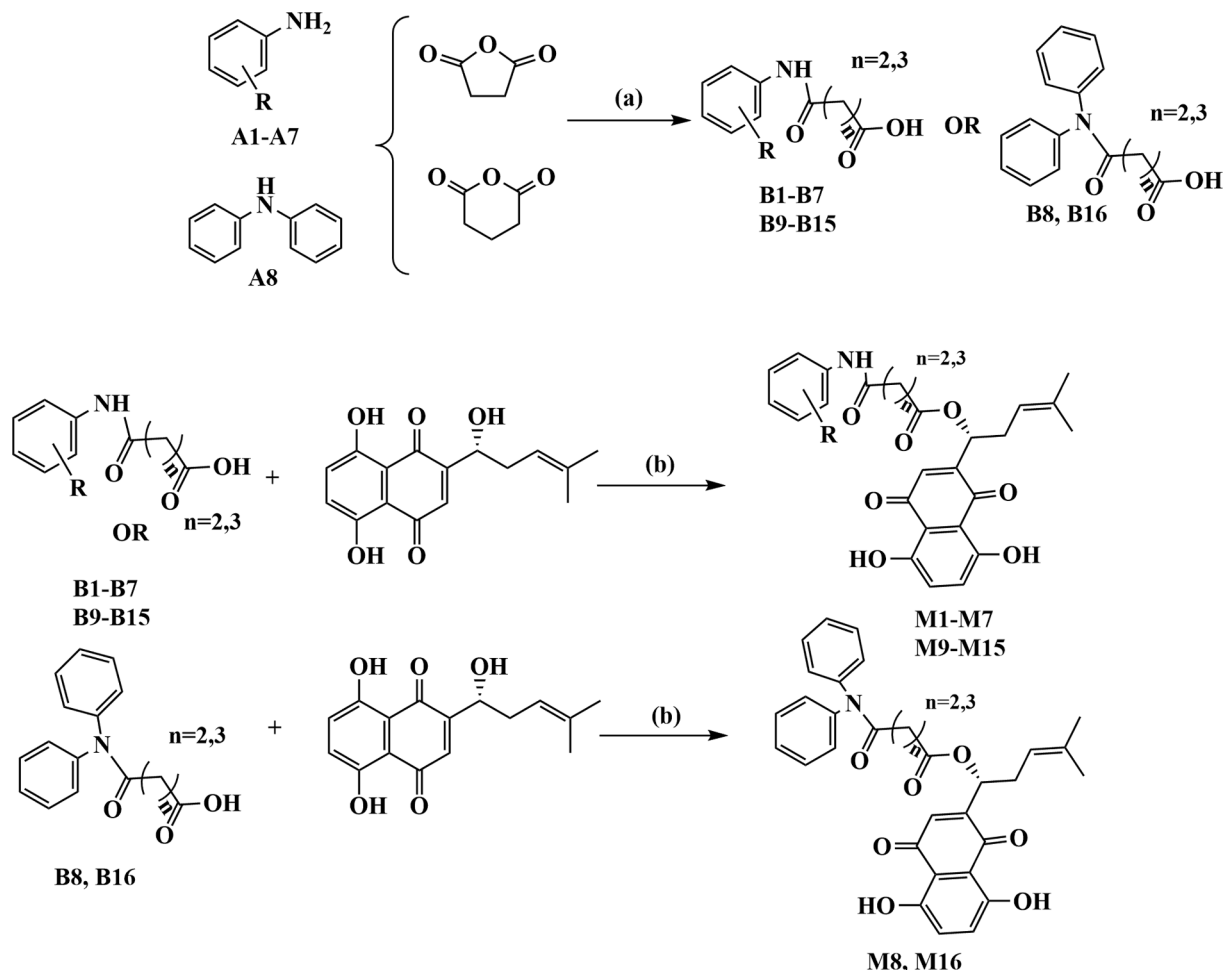
2.3.1. M9 significantly inhibited cancer cell proliferation

Cell Counting Kit-8 (CCK-8) assay were conducted for the anti-proliferative activities by anilide (dicarboxylic acid) shikonin esters M1-M16 against five human cancer cell lines, including two human breast cancer cell lines (MCF-7 and MDA-MB-231), one human cervical cancer cell line (HeLa), one human colon cancer cell line (HCT-8), one human lung adenocarcinoma cell line (A549), and one human normal breast epithelial cell line (MCF-10A). Results shown in Table 2 indicated that all target compounds exhibited good anti-proliferative activity against the five kinds of cancer cell lines, and some of them even showed better inhibitory activity than SK while avoiding MCF-10A, the non-cancer cell line.

Table 1



Compounds	n	R1	R2	R3	R4	R5	R6
M1	2	H	H	H	H	H	H
M2	2	F	H	F	H	H	H
M3	2	F	H	H	H	H	H
M4	2	H	CF ₃	H	H	H	H
M5	2	H	H	Cl	H	H	H
M6	2	H	H	CH ₃	H	H	H
M7	2	CH ₃	H	H	H	H	H
M8	2	H	H	H	H	H	Ph
M9	3	H	H	H	H	H	H
M10	3	F	H	F	H	H	H
M11	3	F	H	H	H	H	H
M12	3	H	CF ₃	H	H	H	H
M13	3	H	H	Cl	H	H	H
M14	3	H	H	CH ₃	H	H	H
M15	3	CH ₃	H	H	H	H	H
M16	3	H	H	H	H	H	Ph



Scheme 1. The synthesis routes of compounds M1-M16. (a) Triethylamine, CH₂Cl₂, room temperature; (b) DCC, DMAP, CH₂Cl₂, ice bath.

Table 2

Inhibition of cell proliferation against five human cancer cell lines (MDA-MB-231, MCF-7, A549, HCT-8, HeLa) and one human normal breast epithelial cell line (MCF-10A) by M1-M16, SK and PTX.

Compounds	IC ₅₀ ± SD (μM)						
	MDA-MB-231	MDA231	MCF-7	A549	HCT-8	Hela	MCF-10A
M1	16.34 ± 2.12		19.55 ± 1.79	21.18 ± 1.68	15.52 ± 0.21	15.92 ± 2.15	83.55 ± 6.59
M2	30.72 ± 2.5		35.6 ± 1.07	41.84 ± 2.3	48.14 ± 2.19	42.45 ± 4.51	88.07 ± 6.83
M3	6.21 ± 1.68		20.15 ± 1.83	7.51 ± 1.04	11.98 ± 0.95	11.35 ± 1.04	78.36 ± 6.4
M4	25.94 ± 1.83		36.43 ± 1.37	28.81 ± 1.19	24.02 ± 2.71	24.06 ± 3.21	52.36 ± 4.95
M5	9.82 ± 2.17		18.01 ± 1.22	28.12 ± 1.15	15.83 ± 1.97	15.35 ± 0.69	61.31 ± 3.67
M6	5.91 ± 1.47		18.26 ± 0.32	12.1 ± 0.73	10.79 ± 1.15	12.83 ± 1.09	55.62 ± 4.42
M7	12.04 ± 1.05		23.34 ± 0.46	16.13 ± 0.32	14.71 ± 0.71	20.66 ± 1.21	88.18 ± 8.45
M8	11.83 ± 1.07		18.63 ± 1.14	13.47 ± 1.18	17.13 ± 1.27	18.5 ± 1.56	61.08 ± 3.12
M9	4.52 ± 0.28		12.21 ± 0.41	6.45 ± 1.11	14.28 ± 1.61	8.77 ± 1.22	>100
M10	38.31 ± 4.31		22.08 ± 1.42	21.08 ± 1.23	13.22 ± 1.52	8.91 ± 1.25	>100
M11	5.13 ± 0.41		11.28 ± 0.81	7.23 ± 1.25	15.98 ± 1.13	9.12 ± 0.87	98.35 ± 7.62
M12	9.12 ± 1.17		17.17 ± 1.51	11.13 ± 1.47	16.48 ± 1.66	18.91 ± 1.28	84.12 ± 6.46
M13	22.9 ± 2.12		26.65 ± 2.25	15.25 ± 1.71	15.09 ± 0.81	17.09 ± 0.19	54.65 ± 5.15
M14	10.54 ± 1.44		19.3 ± 1.14	17.99 ± 1.64	17.72 ± 2.11	13.52 ± 1.28	60.11 ± 3.44
M15	18.19 ± 0.91		30.32 ± 1.21	12.01 ± 0.21	13.97 ± 1.12	17.56 ± 1.84	90.28 ± 5.13
M16	15.19 ± 1.49		25.15 ± 0.79	18.57 ± 0.14	21.9 ± 1.59	26.02 ± 1.17	58.52 ± 4.31
SK	7.62 ± 0.26		9.32 ± 0.17	7.73 ± 0.61	9.2 ± 1.66	11.07 ± 0.17	20.94 ± 1.1
PTX	> 100		0.00416 ± 0.00066	0.00008 ± 0.00002	> 100	0.06219 ± 0.0134	> 100

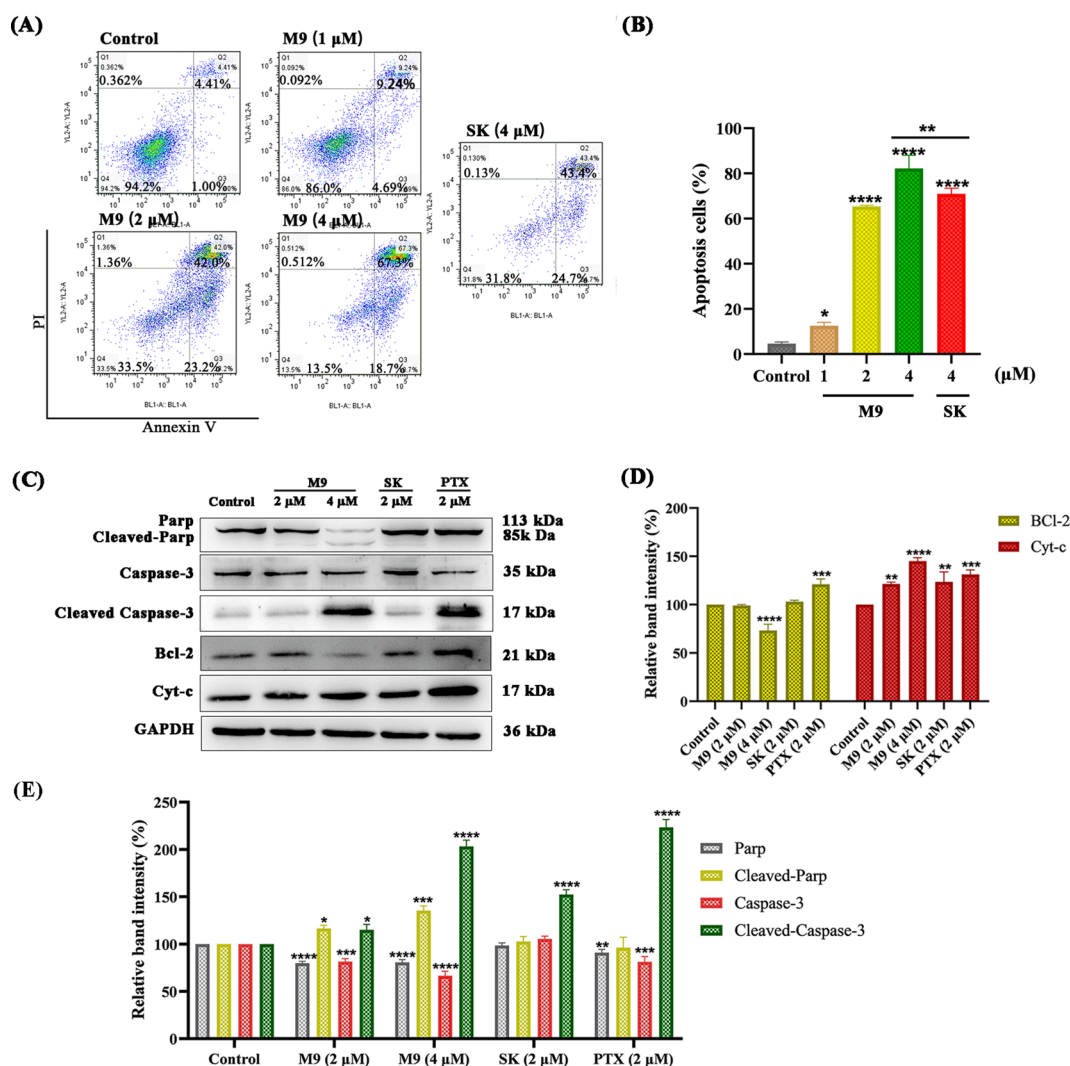


Fig. 2. M9 can induce MDA-MB-231 cell apoptosis. (A) The effect of M9 on cell apoptosis detect by flow cytometry. (B) Statistic analysis of the apoptotic cells detect by flow cytometry. (C) Western blot analysis of the effect of M9 on the expression of apoptosis-related proteins. (D) and (E) The relative band intensity was analyzed by Image J software. The GAPDH band was used as the loading control. The images shown are representative of three repeated experiments. Data shown are mean ± SD of three independent experiments (*P < 0.05, **P < 0.01, ***P < 0.001, ****P < 0.0001).

More specifically, M3 ($IC_{50} = 6.21 \pm 1.68 \mu\text{M}$), M6 ($IC_{50} = 5.91 \pm 1.47 \mu\text{M}$), M9 ($IC_{50} = 4.52 \pm 0.28 \mu\text{M}$) and M11 ($IC_{50} = 5.13 \pm 0.41 \mu\text{M}$) performed better anti-proliferation activities than SK ($IC_{50} = 7.62 \pm 0.26 \mu\text{M}$) and PTX ($IC_{50} > 100 \mu\text{M}$) in MDA-MB-231 cells. For A549 cells, M3 ($IC_{50} = 7.51 \pm 1.04 \mu\text{M}$), M9 ($IC_{50} = 6.45 \pm 1.11 \mu\text{M}$) and M11 ($IC_{50} = 7.23 \pm 1.25 \mu\text{M}$), displayed better anti-proliferation effect than other derivatives and SK ($IC_{50} = 7.73 \pm 0.61 \mu\text{M}$). For HeLa cell line, M9 ($IC_{50} = 8.77 \pm 1.22 \mu\text{M}$), M10 ($IC_{50} = 8.91 \pm 1.25 \mu\text{M}$) and M11 ($IC_{50} = 9.12 \pm 0.87 \mu\text{M}$), showed better anti-proliferation activities than SK ($IC_{50} = 11.07 \pm 0.17 \mu\text{M}$). For MCF-7 and HCT-8 cells, their antiproliferative effect were also significant but slight weaker than that of SK. Moreover, the antiproliferative effect of all target compounds on MCF-10A were obviously weaker than that of cancer cell lines.

Based on the above results, we conjectured that anilide (dicarboxylic acid) shikonin esters intervention could improve the anti-proliferation activities of SK against the cancer cell lines but remarkably reduce its cytotoxicity towards the non-cancer cell line. In order to clarify their potential anticancer mechanism, we chose M9 on MDA-MB-231 cell for further investigation.

2.3.2. M9 can induce apoptosis of MDA-MB-231 cell in a dosage-dependent manner

To further assess the effect of M9 on cell viability, we carried out the apoptosis assay with SK as a positive control. Firstly, MDA-MB-231 cells

were pre-treated with various dosage of M9 (0, 1, 2, 4 μM) and SK (4 μM) for 24 h. Then, using flow cytometer with apoptotic markers to analyze cells for changes in vitro. As shown in Fig. 2 (A and B), the percentage of apoptotic cells in the M9 treated groups increased in a dosage-dependent manner. In addition, M9 can induce more significant cell apoptosis than SK at the same concentration. Further western blot results figure out that M9 could significantly decrease the expression level of the anti-apoptotic proteins (Bcl-2, caspase-3), but increased Cytochrome C (Cyt-C), cleaved-PARP and cleaved-caspase-3 expression in MDA-MB-231 cell line (Fig. 2C, D and E).

2.3.3. Effect of M9 on MDA-MB-231 cell cycle arrest

Next, we assessed the effects of M9 on cell cycle distribution in MDA-MB-231 cells by flow cytometry with SK as a positive control. As shown in Fig. 3 (A, B), M9 caused more and more cell accumulation in S and G₂/M phases in a dosage-dependent manner. To be specific, about 59.15% of cells were arrested in S and G₂/M phases after exposure to 4 μM M9 for 24 h, while about 54.5% cells were arrested at S and G₂/M phases after been exposure to 4 μM SK. Moreover, there was no significant time-dependent effect of M9 on MDA-MB-231 cell cycle arrest. Therefore, we speculated that M9 could not induce cell apoptosis through arresting cell cycle.

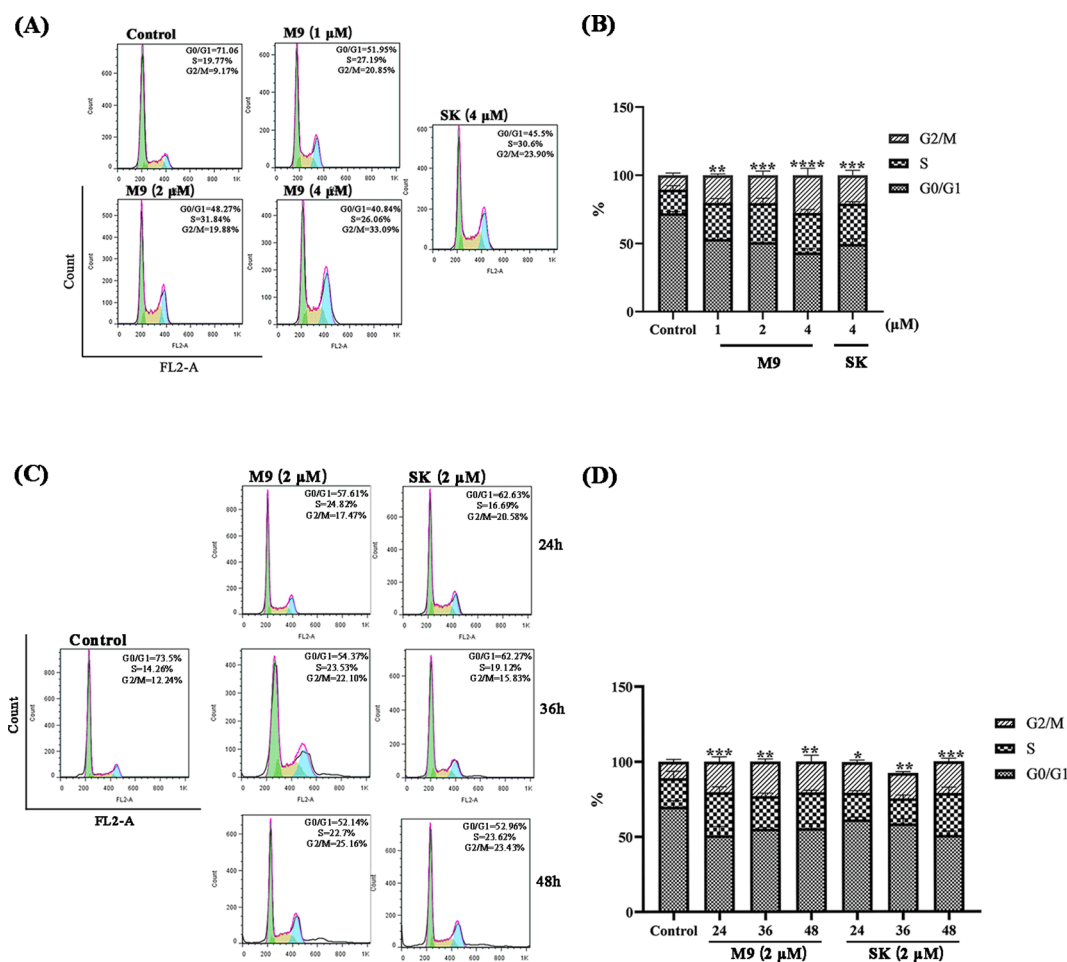


Fig. 3. Effects of M9 and SK on cell cycle distribution of MDA-MB-231 cells. (A) Cell cycle distribution analysis of MDA-MB-231 cells treated with variably dosed M9 and 4 μM SK detect by flow cytometry (G1 phase is color green, S phase is color yellow and G2/M phase is color blue). (B) Statistic analysis of the dosage-dependent assay. (C) Cell cycle distribution analysis of MDA-MB-231 cells after treated with M9 and SK for different time course detect by flow cytometry. (D) Statistic analysis of the time-dependent assay. The images shown are representative of three repeated experiments. Data shown are mean \pm SD of three repeated experiments. (* $P < 0.05$, ** $P < 0.01$, *** $P < 0.001$, **** $P < 0.0001$). (For interpretation of the references to color in this figure legend, the reader is referred to the web version of this article.)

2.3.4. Effect of M9 on cell migration of MDA-MB-231 cells

TNBC is an invasive ductal carcinoma, which is commonly associated with high heterogeneity, low differentiation and rapid proliferation and diffusion [21]. In order to verify the effect of M9 on the migration of MDA-MB-231 cells, we performed wound healing and trans-well assay. As shown in Fig. 4 (A, C), the control group cells gradually occupied the cell-free space in the channel with the passage of time, and the cell channel almost completely healed after 48 h. However, after M9 treatment, the cell scratch healing was significantly slow down in a dosage-dependent manner. Trans-well assay results also indicated that M9 could effectively inhibit cell migration and its effect was much better than SK.

Wnt/ β -catenin signaling pathway plays an important role in many cellular processes, such as cell proliferation and migration. Based on these, we further studied the effect of M9 on Wnt/ β -catenin signaling pathway in MDA-MB-231 cells. Western blot analysis results showed that the expression of β -Catenin and Wnt3a protein was decreased in a dose-dependent manner in MDA-MB-231 cells after being treated with M9 (Fig. 4 D and E). These results suggest that M9 may inhibit the migration of MDA-MB-231 cells by regulating Wnt/ β -catenin signaling pathway.

2.3.5. Effect of M9 on the expression of PI3K/Akt/mTOR in MDA-MB-231 cells

The PI3K/Akt/mTOR signaling pathway are involved in multiple biological processes of cancer progression like cell proliferation, migration and metastasis, etc. [22–24]. As shown in Fig. 5 (A and B), the expression of PI3K, Akt, p-Akt and mTOR was down-regulated in a dose-dependent manner after being treated with M9. Further, we evaluated the effect of M9 on cell proliferation in MDA-MB-231 cells through a colony formation assay [25,26]. The results shown in Fig. 5 (C)

demonstrated that cells incubated in M9 showed lower clone formation rate and smaller clone size than the control group and SK-treated group cells. Moreover, the clone formation inhibitory effect of M9 on MDA-MB-231 cells displayed a dosage-dependent manner. Such results were consistent with the above CCK-8 assay.

2.4. 3d-Qsar analysis

We used 20 compounds, including compounds 1c, 3c and 4c [27] reported in our previous study, for 3D-QSAR study [28]. As shown in Table S1, all test compounds were divided into training set and testing set. The value of R^2 shown in Fig. 6 demonstrated that the model had predictive ability.

In the electrostatic map, the red contour line indicates that the antiproliferative activity is expected to increase in the region of high electron density (negative charge); the blue contour line indicates that the antiproliferative activity is expected to increase in the region of low electron density (partial positive charge). Similarly, the steric map shows green contour lines, which indicate areas where large steric bulk is expected to increase activity, and yellow contour lines indicate areas where small space volume is predicted to decrease activity. The results demonstrated that the compounds with low negative charge and small group of benzene ring had strong anti-proliferative activity Fig. 7. Based on the above data, this model provides reference for the structural optimization of shikonin derivatives that inhibit the proliferation of MDA-MB-231 cells in the subsequent experiments.

3. Conclusion

PI3K/Akt/mTOR signaling pathway plays an important role in the

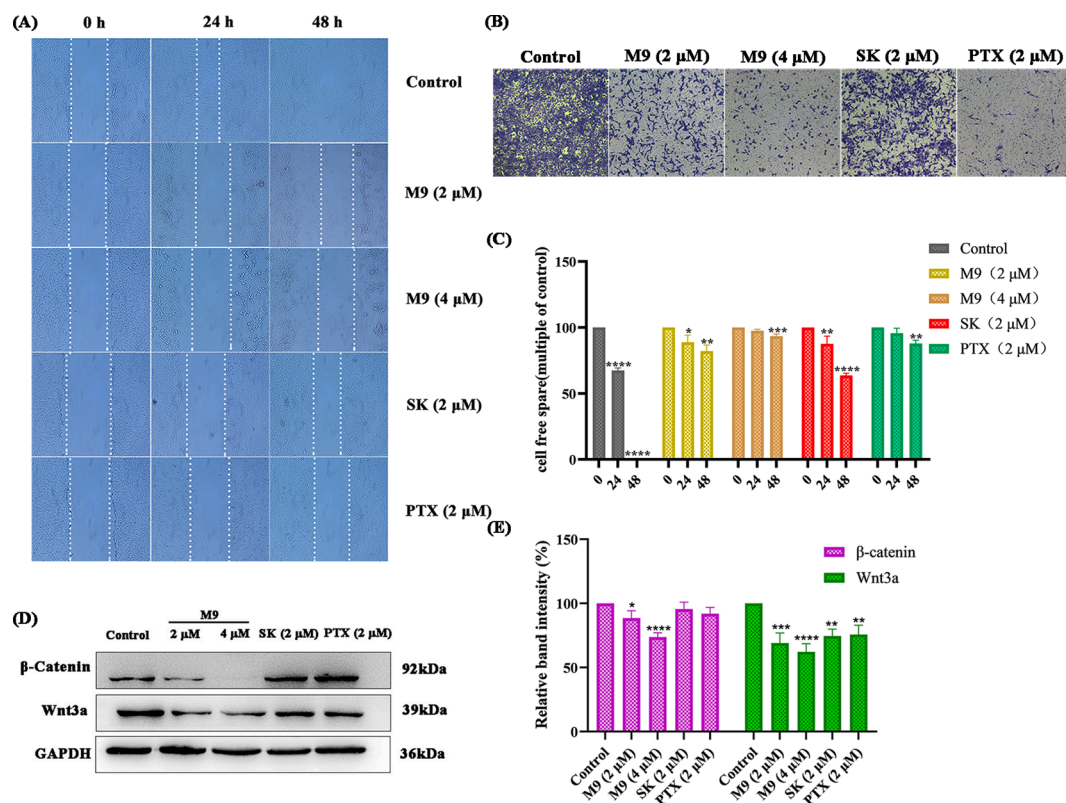


Fig. 4. Effects of M9 on MDA-MB-231 cell migration. (A) Cell migration was detected by wound scratch assay. The representative images of cell migration in the wound scrape model at 0, 24 and 48 h (100 \times). (B) The representative images of trans-well assay at 24 h (100 \times). (C) Statistical analysis of the wound scrape assay. (D) Western blot analysis of the effect of M9 on the expression Wnt and β -catenin. (E) Relative band intensity was analyzed by Image J software. The GAPDH band was used as the loading control. All images shown are representative of three repeated experiments. Data shown are mean \pm SD of three repeated experiments. (* P < 0.05, ** P < 0.01, *** P < 0.001, **** P < 0.0001).

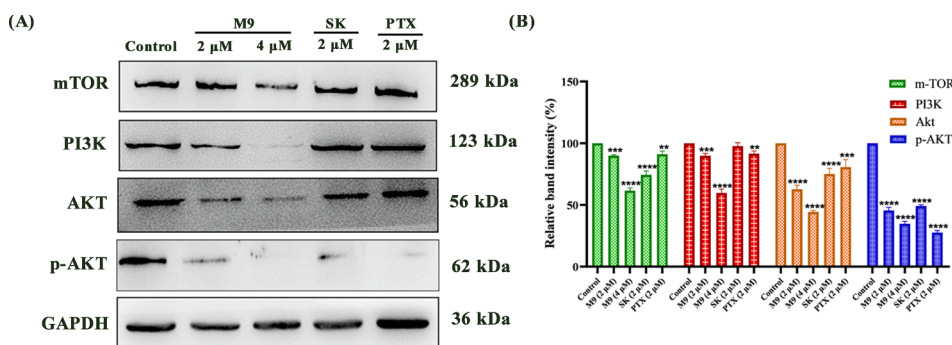


Fig. 5. M9 inhibited MDA-MB-231 cells proliferation by down-regulating the PI3K/Akt/mTOR signaling pathway. (A) Western blot analysis of the effect of M9 on the expression some key proteins in PI3K/Akt/mTOR signaling pathway. (B) Relative band intensity was analyzed by Image J software. The GAPDH band acts as loading control. (C) Colony formation of MDA-MB-231 cells after 7 days of treatment with different concentrations of M9. The images shown are representative of three repeated experiments. Data shown are mean \pm SD of three repeated experiments. (**P < 0.01, ***P < 0.001, ****P < 0.0001).

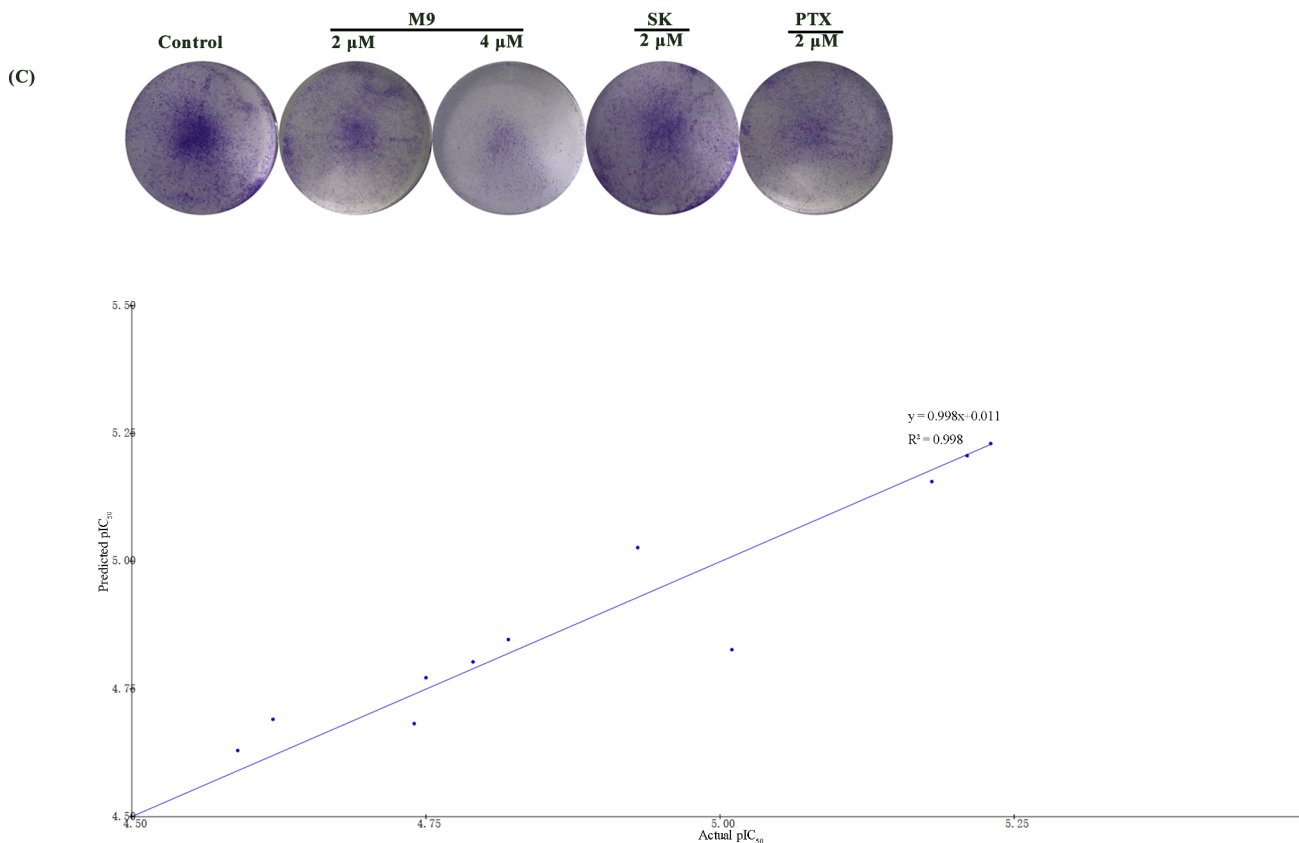


Fig. 6. The experimental and predicted anti-proliferative activity curves of training set and test set.

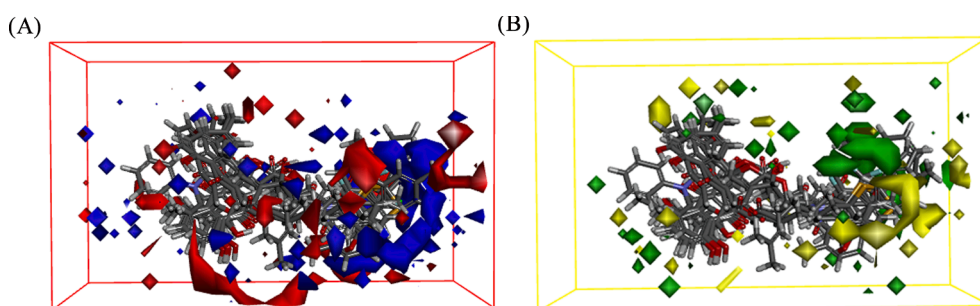


Fig. 7. (A) 3D-QSAR model coefficients on electrostatic potential grids. (B) 3D-QSAR model coefficients on van der Waals grids. The blue and green sections represent positive coefficients; the red and yellow sections represent negative coefficients. (For interpretation of the references to color in this figure legend, the reader is referred to the web version of this article.)

research of antitumor drugs [29]. In this study, the pharmacophore structure of aniline was introduced into the shikonin framework, and a series of anilide (dicarboxylic acid) shikonin ester were obtained. The antiproliferative activity showed that M9 had the best inhibitory activity against MDA-MB-231 cells. Western blot results showed that M9 facilitate the expression of some pro-apoptotic proteins, such as cleaved-caspase-3, cytochrome C, and cleaved-PARP. Further studies have shown that M9 can cause cell cycle arrest, but the effect is not significant. Moreover, M9 could negatively regulate the PI3K/Akt/mTOR signaling pathway and eventually lead to dose-dependent apoptosis in MDA-MB-231 cells. Meanwhile, the inhibition of migration of MDA-MB-231 cell may effectively reduce the possibility of distal metastasis. The wound scrape and Trans-well assay suggested that M9 might further inhibit the migration of MDA-MB-231 cells through the inhibition of Wnt/ β -catenin signaling pathway. Molecular docking results demonstrated that M9 could bind well to the active site of Akt (PDB code: 3CQW) by forming various binding interactions, thus promoting its antitumor effect. Therefore, we can speculate that M9 may have great potential in the development of anti-breast cancer drugs by targeting PI3K/AKT/mTOR signaling pathway.

4. Methods

4.1. Materials and measurements

All chemical reagents or solvents used to synthesize compounds are analytical grade and purchased from Nanjing Chemical CO. Ltd (China) and Sigma-Aladdin (St. Louis, USA). All the ^1H NMR and ^{13}C NMR spectra were recorded on a Bruker DPX 600 model spectrometer in d^6 -DMSO or CDCl_3 . The chemical shifts (δ) for ^1H NMR and ^{13}C NMR spectra were reported in ppm(δ), with TMS as an internal standard. The ESI-MS spectra were obtained on a Mariner Biospectrometry Workstation (ESI-TOF) mass spectrometer (4600 UPLC/Triple). The melting point (uncorrected) was detected by using a XT4 MP Apparatus (Taikang Corp., Beijing, China). Column chromatography was conducted by using silica gel (200–300 mesh) and eluting with ethyl acetate, dichloromethane and petroleum ether (bp 30–60 °C). Thin layer chromatography (TLC) was carried out on glass-backed silica gel plates (Silica Gel 60 Å GF254) and visualized in UV light (λ 254 nm).

PTX was purchased from Sigma-Aldrich (St. Louis, USA). RIPA lysis buffers (P0013B) was purchased from Beyotime (Shanghai, China). PVDF membranes were purchased from Thermo Scientific. Protease inhibitor cocktail I (C0001) and phosphatase inhibitor cocktail I (C0002) were purchased from Target Mol (Boston, USA). BCA protein assay kit (#23227) was purchased from Pierce (Rockford, IL, USA). Anti-Cytochrome C (10993-1-AP) was purchased from Proteintech (Wuhan, China); anti-wnt3a (ab219412) was purchased from Abcom. (Cambridge, UK). Anti- β -Catenin (66379-2-Ig), anti-GAPDH (60004-1-Ig), anti-PARP (66520-1-Ig), anti-Bcl-2 (60178-1-Ig), anti-PI3K (67121-1-Ig), anti-Akt (60203-2-Ig), anti-p-Akt (66444-Ig), anti-mTOR (66888-1-Ig), the secondary antibody goat anti-mouse IgG (H + L) (SA00001-1), goat anti-rabbit IgG (H + L) (SA00001-2) were purchased from Proteintech (Wuhan, China). Anti-Caspase-3 (WL02117), anti-cleaved caspase-3 (WL03089) were purchased from Wanlei Biotech Co. Ltd (Shenyang, China). CCK-8, Cell cycle, Annexin V-FITC cell apoptosis assay kits and ECL detection kit were purchased from YEASEN Biotech Co. Ltd (Shanghai, China).

4.2. General procedure for the synthesis of compounds B1-B16

All the compounds were listed in Table 1 and their synthesis routes were outlined in Scheme 1. Aniline (1 mol) and succinic anhydride OR glutaric anhydride (1 mol), glutaric anhydride (1 mol) were put into a 50 mL conical flask. Then, add 20 mL of anhydrous dichloromethane to make them dissolved. The appropriate amount of triethylamine was used as catalyst. The reaction system was stirred at room temperature

for 6 h and monitored by thin layer chromatography (TLC). When the reaction is completed, the pure intermediate B1-B16 was obtained by filtered and recrystallization.

4.3. General procedure for the synthesis of compounds M1-M16

Compounds M1-M16 (0.2 mmol) was dissolved in anhydrous dichloromethane (20 mL) at room temperature. Then, 0.4 mmol dicyclohexylcarbodiimide (DCC) and 0.05 mmol 4-dimethylaminopyridine (DMAP) was added and stirred for 0.5 h. After that, 0.2 mmol of shikonin was added to the reaction mixture and stirred in the ice bath for over 4 h. The solvent was then removed by rotary evaporation and the residue was purified by silica gel column chromatography (with ethyl acetate: petroleum ether, the specific proportion is shown in Table S2) to get target compounds (Scheme 1). Chemical structures of the target compounds (M1-M16) shown in Table 1.

(R)-1-(5,8-dihydroxy-1,4-dioxo-1,4-dihydronaphthalen-2-yl)-4-methylpent-3-en-1-yl 4-oxo-4-(phenylamino) butanoate (M1)

Red powders, yield 53%. Mp: 79.1–80.3 °C. ^1H NMR (600 MHz, CDCl_3) δ 12.58 (d, J = 4.6 Hz, 1H), 12.42 (d, J = 4.7 Hz, 1H), 7.49 (t, J = 7.8 Hz, 3H), 7.41 (t, J = 7.5 Hz, 1H), 7.29 (dd, J = 7.3, 5.3 Hz, 3H), 7.17 (s, 1H), 7.05 (s, 1H), 6.09–6.00 (m, 1H), 5.11 (t, J = 7.2 Hz, 1H), 2.86–2.80 (m, 2H), 2.70–2.64 (m, 2H), 2.63–2.57 (m, 1H), 2.49 (dt, J = 14.8, 7.3 Hz, 1H), 1.65 (d, J = 17.4 Hz, 3H), 1.56 (s, 3H). ^{13}C NMR (151 MHz, CDCl_3) δ 177.77 (s), 176.26 (s), 172.44 (s), 169.54 (s), 168.03 (s), 167.50 (s), 148.13 (s), 138.17 (s), 132.82 (s), 131.64 (s), 129.24 (s), 128.97 (s), 128.71 (s), 126.47 (s), 124.29 (s), 119.66 (s), 117.48 (s), 111.81–111.80 (m), 111.58 (s), 70.04 (s), 33.87 (s), 28.43 (s), 25.57 (s), 24.90 (s), 17.97 (s). HRESIMS [M+H]⁺ + m/z 463.1588 (Calcd for $\text{C}_{26}\text{H}_{25}\text{NO}_7$ 463.1631).

(R)-1-(5,8-dihydroxy-1,4-dioxo-1,4-dihydronaphthalen-2-yl)-4-methylpent-3-en-1-yl 4-((2,4-difluorophenyl) amino)-4-oxobutanoate (M2)

Red powders, yield 72%. Mp: 57.8–58.7 °C. ^1H NMR (600 MHz, CDCl_3) δ 12.58 (s, 1H), 12.43 (s, 1H), 7.44 (d, J = 9.7 Hz, 2H), 7.21–7.15 (m, 3H), 7.05 (s, 2H), 6.07–6.01 (m, 1H), 5.14–5.09 (m, 1H), 2.86–2.83 (m, 2H), 2.72 (dd, J = 10.6, 5.9 Hz, 2H), 2.53–2.47 (m, 2H), 1.67 (d, J = 6.3 Hz, 3H), 1.57 (s, 3H). ^{13}C NMR (151 MHz, CDCl_3) δ 177.83 (s), 176.31 (s), 175.24 (s), 171.77 (s), 169.35 (s), 167.77 (s), 163.06 (dd, J = 250.5, 12 Hz), 157.69 (dd, J = 253.5, 12 Hz), 147.64 (s), 136.24 (s), 132.99 (s), 132.78 (s), 131.64 (s), 130.20 (d, J = 10.5 Hz), 117.49 (s), 112.08 (dd, J = 22.5, 3 Hz), 111.78 (s), 105.31 (dd, J = 25.5, 22.5 Hz), 70.10 (s), 33.75 (s), 32.76 (s), 28.52 (s), 24.85 (s), 17.95 (s). HRESIMS [M+H]⁺ + m/z 499.1393 (Calcd for $\text{C}_{26}\text{H}_{23}\text{F}_2\text{NO}_7$ 499.1443).

(R)-1-(5,8-dihydroxy-1,4-dioxo-1,4-dihydronaphthalen-2-yl)-4-methylpent-3-en-1-yl 4-((2-fluorophenyl) amino)-4-oxobutanoate (M3)

Red powders, yield 68%. Mp: 66.5–68.1 °C. ^1H NMR (600 MHz, CDCl_3) δ 12.58 (s, 1H), 12.43 (s, 1H), 8.29 (t, J = 7.8 Hz, 1H), 7.54 (s, 1H), 7.20–7.15 (m, 2H), 7.13–7.00 (m, 4H), 6.09–6.01 (m, 1H), 5.12 (t, J = 7.2 Hz, 1H), 2.85 (t, J = 6.4 Hz, 2H), 2.73 (dd, J = 13.0, 6.8 Hz, 2H), 2.62 (dd, J = 12.2, 6.1 Hz, 1H), 2.50 (dt, J = 14.7, 7.3 Hz, 1H), 1.65 (d, J = 26.8 Hz, 3H), 1.55 (d, J = 21.3 Hz, 3H). ^{13}C NMR (151 MHz, CDCl_3) δ 177.96 (s), 176.46 (s), 171.76 (s), 169.34 (s), 167.67 (s), 167.15 (s), 152.20 (d, J = 243 Hz), 147.71 (s), 136.25 (s), 132.95 (s), 132.75 (s), 131.70 (s), 124.58 (d, J = 3.6 Hz), 124.31 (d, J = 7.6 Hz), 121.65 (s), 117.52 (s), 114.72 (d, J = 19 Hz), 111.70 (d, J = 33 Hz), 70.08 (s), 32.78 (s), 31.96 (s), 29.31 (s), 25.74 (s), 17.97 (s). HRESIMS [M+H]⁺ + m/z 481.1492 (Calcd for $\text{C}_{26}\text{H}_{24}\text{FNO}_7$ 481.1537).

(R)-1-(5,8-dihydroxy-1,4-dioxo-1,4-dihydronaphthalen-2-yl)-4-methylpent-3-en-1-yl 4-oxo-4-((3-(trifluoromethyl) phenyl) amino) butanoate (M4)

Red powders, yield 65%. Mp: 71.2–72.5 °C. ^1H NMR (600 MHz, CDCl_3) δ 12.60 (d, J = 18.6 Hz, 1H), 12.41 (s, 1H), 7.53 (d, J = 8.0 Hz, 4H), 7.33 (d, J = 7.2 Hz, 1H), 7.20–7.14 (m, 2H), 7.06 (s, 1H), 6.08–6.02 (m, 1H), 5.11 (t, J = 7.0 Hz, 1H), 2.86–2.78 (m, 3H), 2.71 (s, 2H),

2.53–2.46 (m, 1H), 1.66 (s, 3H), 1.57 (s, 3H). ^{13}C NMR (151 MHz, CDCl_3) δ 177.46 (s), 175.70 (s), 172.07 (s), 169.70 (s), 167.89 (s), 147.51 (s), 138.40 (s), 136.33 (s), 133.03 (d, $J = 37.5$ Hz), 132.38 (s), 131.58 (d, $J = 7.5$ Hz), 129.77 (s), 129.46 (s), 124.46 (q, $J = 279$ Hz), 120.81–120.60 (m), 117.46 (s), 116.54–116.23 (m), 111.80 (s), 111.56 (s), 70.16 (s), 33.71 (s), 30.75 (s), 28.41 (s), 24.84 (s), 17.97 (s). HRESIMS [M+H]⁺ m/z 531.1467 (Calcd for $\text{C}_{27}\text{H}_{24}\text{F}_3\text{NO}_7$ 531.1505).

(R)-1-(5,8-dihydroxy-1,4-dioxo-1,4-dihydronaphthalen-2-yl)-4-methylpent-3-en-1-yl 4-((4-chlorophenyl) amino)-4-oxobutanoate (M5)

Red powders, yield 58%. Mp: 74.2–75.4 °C. ^1H NMR (600 MHz, CDCl_3) δ 12.56 (d, $J = 18.7$ Hz, 1H), 12.42 (s, 1H), 7.69 (s, 1H), 7.45 (dd, $J = 8.7, 1.9$ Hz, 3H), 7.23 (s, 1H), 7.20–7.15 (m, 2H), 7.04 (s, 1H), 6.08–6.01 (m, 1H), 5.11 (t, $J = 7.1$ Hz, 1H), 2.86–2.79 (m, 2H), 2.71–2.64 (m, 2H), 2.49 (dt, $J = 14.8, 7.3$ Hz, 2H), 1.66 (s, 3H), 1.56 (s, 3H). ^{13}C NMR (151 MHz, CDCl_3) δ 177.54 (s), 175.99 (s), 172.28 (s), 170.19 (s), 168.11 (s), 167.58 (s), 148.01 (s), 137.77 (s), 136.28 (s), 133.14 (s), 132.99 (s), 131.26 (s), 128.99 (s), 124.29 (s), 119.74 (s), 117.59 (s), 111.80 (s), 111.56 (s), 69.64 (s), 36.21 (s), 33.09 (s), 32.84 (s), 25.98 (s), 20.89 (s), 17.98 (s). HRESIMS [M+H]⁺ m/z 497.1200 (Calcd for $\text{C}_{26}\text{H}_{24}\text{ClNO}_7$ 497.1241)

(R)-1-(5,8-dihydroxy-1,4-dioxo-1,4-dihydronaphthalen-2-yl)-4-methylpent-3-en-1-yl 4-oxo-4-(p-tolylamino) butanoate (M6)

Red powders, yield 55%. Mp: 98.7–100.2 °C. ^1H NMR (600 MHz, CDCl_3) δ 12.58 (s, 1H), 12.42 (s, 1H), 7.39 (d, $J = 17.2$ Hz, 1H), 7.35 (d, $J = 8.0$ Hz, 1H), 7.19–7.13 (m, 3H), 7.11–7.02 (m, 3H), 6.08–6.01 (m, 1H), 5.11 (t, $J = 6.6$ Hz, 1H), 2.90 (s, 3H), 2.70–2.58 (m, 3H), 2.29 (s, 3H), 1.66 (s, 3H), 1.56 (s, 3H). ^{13}C NMR (151 MHz, CDCl_3) δ 177.81 (s), 176.41 (s), 172.03 (s), 169.13 (s), 167.78 (s), 167.26 (s), 147.69 (s), 136.28 (s), 131.66 (s), 129.91 (s), 129.44 (s), 126.28 (s), 119.75 (s), 117.49 (s), 111.80 (s), 111.57 (s), 70.00 (s), 33.76 (s), 32.80 (s), 28.41 (s), 24.85 (s), 21.22 (s), 17.97 (s). HRESIMS [M+H]⁺ m/z 477.1744 (Calcd for $\text{C}_{27}\text{H}_{27}\text{NO}_7$ 477.1788).

(R)-1-(5,8-dihydroxy-1,4-dioxo-1,4-dihydronaphthalen-2-yl)-4-methylpent-3-en-1-yl 4-oxo-4-(o-tolylamino)butanoate (M7)

Red powders, yield 61%. Mp: 80.6–81.4 °C. ^1H NMR (600 MHz, CDCl_3) δ 12.59 (s, 1H), 12.41 (s, 1H), 7.78 (dd, $J = 29.8, 7.6$ Hz, 2H), 7.33 (ddd, $J = 21.9, 15.1, 7.5$ Hz, 1H), 7.22–7.12 (m, 3H), 7.10–7.03 (m, 2H), 6.11–6.01 (m, 1H), 5.11 (t, $J = 7.2$ Hz, 1H), 2.91–2.82 (m, 2H), 2.71 (t, $J = 6.5$ Hz, 2H), 2.65–2.59 (m, 1H), 2.53–2.46 (m, 1H), 2.24–2.12 (m, 3H), 1.67 (s, 3H), 1.57 (s, 3H). ^{13}C NMR (151 MHz, CDCl_3) δ 177.58 (s), 176.21 (s), 172.12 (s), 169.46 (s), 167.98 (s), 167.45 (s), 156.82 (s), 147.62 (s), 136.31 (s), 135.54 (s), 133.08 (s), 132.84 (s), 130.41 (s), 129.63 (s), 127.93 (s), 125.16 (s), 122.95 (s), 117.45 (s), 111.79 (s), 111.55 (s), 70.01 (s), 33.87 (s), 32.79 (s), 25.49 (s), 24.90 (s), 17.95 (s), 17.74 (s). HRESIMS [M+H]⁺ m/z 477.1743 (Calcd for $\text{C}_{27}\text{H}_{27}\text{NO}_7$ 477.1788).

(R)-1-(5,8-dihydroxy-1,4-dioxo-1,4-dihydronaphthalen-2-yl)-4-methylpent-3-en-1-yl 4-(diphenylamino)-4-oxobutanoate (M8)

Red oil, yield 51%. ^1H NMR (600 MHz, CDCl_3) δ 12.58 (s, 1H), 12.44 (s, 1H), 7.50 (s, 1H), 7.43 (d, $J = 6.5$ Hz, 3H), 7.35 (d, $J = 12.7$ Hz, 4H), 7.21–7.16 (m, 4H), 7.03 (s, 1H), 6.07–5.94 (m, 1H), 5.11 (t, $J = 7.1$ Hz, 1H), 2.78–2.71 (m, 2H), 2.66 (d, $J = 6.6$ Hz, 2H), 2.55 (t, $J = 6.6$ Hz, 2H), 1.66 (s, 3H), 1.55 (s, 3H). ^{13}C NMR (151 MHz, CDCl_3) δ 177.54 (s), 175.99 (s), 172.28 (s), 170.19 (s), 168.11 (s), 167.58 (s), 148.01 (s), 137.77 (s), 136.28 (s), 133.14 (s), 132.99 (s), 131.26 (s), 128.99 (s), 124.29 (s), 119.74 (s), 117.59 (s), 111.80 (s), 111.56 (d, $J = 4.3$ Hz), 69.64 (s), 36.21 (s), 33.09 (s), 32.84 (s), 25.98 (s), 20.89 (s), 17.98 (s). HRESIMS [M+H]⁺ m/z 539.1936 (Calcd for $\text{C}_{32}\text{H}_{29}\text{NO}_7$ 539.1944).

(R)-1-(5,8-dihydroxy-1,4-dioxo-1,4-dihydronaphthalen-2-yl)-4-methylpent-3-en-1-yl 5-oxo-5-(phenylamino) pentanoate (M9)

Red powders, yield 55%. Mp: 46.2–47.1 °C. ^1H NMR (600 MHz, CDCl_3) δ 12.60 (s, 1H), 12.42 (s, 1H), 7.51 (d, $J = 7.9$ Hz, 2H), 7.41 (dd, $J = 22.0, 12.6$ Hz, 1H), 7.30 (t, $J = 7.7$ Hz, 2H), 7.20–7.16 (m, 2H), 7.09 (t, $J = 6.9$ Hz, 1H), 6.99 (s, 1H), 6.09–6.00 (m, 1H), 5.12 (t, $J = 6.7$ Hz, 1H), 2.65–2.39 (m, 6H), 2.12–2.04 (m, 2H), 1.68 (s, 3H), 1.58 (s, 3H).

^{13}C NMR (151 MHz, CDCl_3) δ 177.54 (s), 175.99 (s), 172.28 (s), 170.19 (s), 168.11 (s), 167.58 (s), 148.01 (s), 137.77 (s), 136.28 (s), 133.14 (s), 132.99 (s), 131.26 (s), 128.99 (s), 124.29 (s), 119.74 (s), 117.59 (s), 111.80 (s), 111.56 (s), 69.64 (s), 36.21 (s), 33.09 (s), 32.84 (s), 25.98 (s), 20.89 (s), 17.98 (s). HRESIMS [M+H]⁺ m/z 477.1746 (Calcd for $\text{C}_{27}\text{H}_{27}\text{NO}_7$ 477.1788).

(R)-1-(5,8-dihydroxy-1,4-dioxo-1,4-dihydronaphthalen-2-yl)-4-methylpent-3-en-1-yl 5-((2,4-difluorophenyl) amino)-5-oxopentanoate (M10)

Red powders, yield 71%. Mp: 61.8–62.6 °C. ^1H NMR (600 MHz, CDCl_3) δ 12.62–12.56 (m, 1H), 12.45–12.37 (m, 1H), 8.26–8.17 (m, 1H), 7.34 (s, 1H), 7.22–7.14 (m, 2H), 7.00 (s, 1H), 6.90–6.82 (m, 2H), 6.05 (dd, $J = 6.9, 4.8$ Hz, 1H), 5.13 (dd, $J = 18.0, 10.8$ Hz, 1H), 2.58–2.51 (m, 2H), 2.51–2.44 (m, 3H), 2.18 (s, 1H), 2.13–2.04 (m, 2H), 1.67 (d, $J = 15.5$ Hz, 3H), 1.58 (s, 3H). ^{13}C NMR (151 MHz, CDCl_3) δ 177.49 (s), 175.96 (s), 172.02 (s), 170.29 (s), 162.78 (dd, $J = 249, 12$ Hz), 157.87 (dd, $J = 250.5, 12$ Hz), 147.94 (s), 136.26 (s), 133.15 (s), 132.98 (s), 131.30 (s), 131.15 (d, $J = 10.5$ Hz), 117.61 (s), 111.80 (dd, $J = 22.5, 3$ Hz), 111.81 (s), 111.56 (s), 104.93 (dd, $J = 27, 24$ Hz), 69.60 (s), 35.95 (s), 32.80 (s), 25.77 (s), 25.58 (s), 20.47 (s), 17.97 (s). HRESIMS [M+H]⁺ m/z 513.1557 (Calcd for $\text{C}_{27}\text{H}_{25}\text{F}_2\text{NO}_7$ 513.1599).

(R)-1-(5,8-dihydroxy-1,4-dioxo-1,4-dihydronaphthalen-2-yl)-4-methylpent-3-en-1-yl 5-((2-fluorophenyl) amino)-5-oxopentanoate (M11)

Red powders, yield 67%. Mp: 67.5–68.8 °C. ^1H NMR (600 MHz, CDCl_3) δ 12.60 (d, $J = 8.8$ Hz, 1H), 12.42 (s, 1H), 8.29 (t, $J = 7.8$ Hz, 1H), 7.44 (s, 1H), 7.22–7.15 (m, 2H), 7.14–6.96 (m, 4H), 6.05 (dd, $J = 6.8, 4.8$ Hz, 1H), 5.15–5.08 (m, 1H), 2.68–2.43 (m, 7H), 2.12–2.06 (m, 2H), 1.73–1.64 (m, 3H), 1.56 (d, $J = 20.7$ Hz, 3H). ^{13}C NMR (151 MHz, CDCl_3) δ 177.57 (s), 176.05 (s), 172.03 (s), 170.26 (s), 168.08 (s), 167.55 (s), 152.34 (d, $J = 241.5$ Hz), 147.96 (s), 136.27 (s), 133.12 (s), 132.94 (s), 131.35 (s), 124.58 (d, $J = 3.5$ Hz), 124.38 (d, $J = 7.6$ Hz), 121.80 (s), 117.61 (s), 114.80 (d, $J = 19.5$ Hz), 111.70 (d, $J = 36$ Hz), 69.59 (s), 36.17 (s), 33.06 (s), 32.86 (s), 25.77 (s), 20.48 (s), 17.97 (s). HRESIMS [M+H]⁺ m/z 495.1646 (Calcd for $\text{C}_{27}\text{H}_{26}\text{FNO}_7$ 495.1693).

(R)-1-(5,8-dihydroxy-1,4-dioxo-1,4-dihydronaphthalen-2-yl)-4-methylpent-3-en-1-yl 5-oxo-5-((3-(trifluoromethyl) phenyl) amino) pentanoate (M12)

Red powders, yield 63%. Mp: 44.7–45.6 °C. ^1H NMR (600 MHz, CDCl_3) δ 12.60 (d, $J = 8.8$ Hz, 1H), 12.42 (s, 1H), 8.29 (t, $J = 7.8$ Hz, 1H), 7.44 (s, 1H), 7.22–7.15 (m, 2H), 7.14–6.96 (m, 4H), 6.05 (dd, $J = 6.8, 4.8$ Hz, 1H), 5.15–5.08 (m, 1H), 2.68–2.43 (m, 6H), 2.12–2.06 (m, 2H), 1.73–1.64 (m, 3H), 1.56 (d, $J = 20.7$ Hz, 4H). ^{13}C NMR (151 MHz, CDCl_3) δ 177.39 (s), 175.82 (s), 172.31 (s), 170.47 (s), 168.31 (s), 167.78 (s), 147.94 (s), 138.36 (s), 136.34 (s), 133.16 (d, $J = 20.5$ Hz), 131.19 (d), 129.77 (s), 129.52 (s), 123.82 (q, $J = 273$ Hz), 120.94–120.70 (m), 117.55 (s), 116.55–116.24 (m), 111.81 (s), 111.57 (s), 69.75 (s), 36.12 (s), 33.02 (s), 32.83 (s), 25.78 (s), 20.57 (s), 17.98 (s). HRESIMS [M+H]⁺ m/z 545.1622 (Calcd for $\text{C}_{28}\text{H}_{26}\text{F}_3\text{NO}_7$ 545.1661)

(R)-1-(5,8-dihydroxy-1,4-dioxo-1,4-dihydronaphthalen-2-yl)-4-methylpent-3-en-1-yl 5-((4-chlorophenyl) amino)-5-oxopentanoate (M13)

Red powders, yield 60%. Mp: 65.8–67.1 °C. ^1H NMR (600 MHz, CDCl_3) δ 12.60 (s, 1H), 12.42 (s, 1H), 7.57–7.40 (m, 4H), 7.20 (d, $J = 10.0$ Hz, 2H), 7.05–6.95 (m, 2H), 6.06–6.01 (m, 1H), 5.09 (dd, $J = 28.9, 22.1$ Hz, 2H), 2.88–2.75 (m, 2H), 2.57–2.50 (m, 2H), 2.43 (dd, $J = 16.5, 7.4$ Hz, 2H), 2.07 (dd, $J = 14.2, 7.1$ Hz, 2H), 1.67 (d, $J = 13.2$ Hz, 3H), 1.58 (s, 3H). ^{13}C NMR (151 MHz, CDCl_3) δ 177.62 (s), 176.21 (s), 172.33 (s), 170.61 (s), 168.42 (s), 157.46 (s), 147.96 (s), 136.33 (s), 133.22 (s), 133.08 (s), 131.21 (s), 129.84 (s), 129.54 (s), 128.98 (s), 120.94 (s), 117.56 (s), 111.86 (s), 111.56 (s), 69.70 (s), 36.16 (s), 33.80 (s), 32.82 (s), 25.54 (s), 24.87 (s), 17.98 (s). HRESIMS [M+H]⁺ m/z 511.1353 (Calcd for $\text{C}_{27}\text{H}_{26}\text{ClNO}_7$ 511.1398)

(R)-1-(5,8-dihydroxy-1,4-dioxo-1,4-dihydronaphthalen-2-yl)-4-methylpent-3-en-1-yl 5-oxo-5-(p-tolylamino) pentanoate (M14)

Red powders, yield 53%. Mp: 83.5–84.1 °C. ^1H NMR (600 MHz, CDCl_3) δ 12.60 (s, 1H), 12.42 (d, $J = 4.9$ Hz, 1H), 7.39 (d, $J = 8.3$ Hz, 2H), 7.27 (d, $J = 8.8$ Hz, 1H), 7.21–7.15 (m, 2H), 7.15–7.07 (m, 2H), 7.01–6.95 (m, 1H), 6.04 (dd, $J = 6.9, 4.8$ Hz, 1H), 5.11 (t, $J = 7.1$ Hz, 1H), 2.56–2.45 (m, 3H), 2.45–2.34 (m, 3H), 2.30 (s, 2H), 2.14–1.99 (m, 3H), 1.68 (s, 3H), 1.59 (d, $J = 12.6$ Hz, 3H). ^{13}C NMR (151 MHz, CDCl_3) δ 177.63 (s), 176.09 (s), 172.28 (s), 170.05 (s), 168.05 (s), 167.52 (s), 148.04 (s), 136.28 (s), 135.20 (s), 133.94 (s), 133.11 (s), 132.95 (s), 131.29 (s), 129.47 (s), 119.85 (s), 117.60 (s), 111.82 (s), 111.58 (s), 69.62 (s), 36.17 (s), 33.12 (s), 32.85 (s), 25.78 (s), 20.86 (s), 20.72 (s), 17.98 (s). HRESIMS $[\text{M}+\text{H}]^+ m/z$ 491.1903 (Calcd for $\text{C}_{28}\text{H}_{29}\text{NO}_7$ 491.1944).

(R)-1-(5,8-dihydroxy-1,4-dioxo-1,4-dihydronaphthalen-2-yl)-4-methylpent-3-en-1-yl 5-oxo-5-(o-tolylamino) pentanoate (M15)

Red powders, yield 59%. Mp: 58.2–59.2 °C. ^1H NMR (600 MHz, CDCl_3) δ 12.60 (s, 1H), 12.41 (s, 1H), 7.78 (d, $J = 7.9$ Hz, 1H), 7.24–7.15 (m, 4H), 7.14–7.04 (m, 2H), 7.00 (s, 1H), 6.10–6.02 (m, 1H), 5.11 (d, $J = 6.5$ Hz, 1H), 2.59 (ddd, $J = 19.6, 14.0, 7.8$ Hz, 3H), 2.52–2.44 (m, 3H), 2.24 (d, $J = 16.0$ Hz, 3H), 2.11 (dd, $J = 19.9, 12.9$ Hz, 2H), 1.69 (s, 3H), 1.58 (s, 3H). ^{13}C NMR (151 MHz, CDCl_3) δ 177.20 (s), 175.68 (s), 171.91 (s), 169.98 (s), 167.88 (s), 167.35 (s), 147.66 (s), 136.00 (s), 135.20 (s), 132.87 (s), 132.69 (s), 131.01 (s), 130.21 (s), 126.46 (s), 125.01 (s), 122.95 (s), 117.31 (s), 111.52 (s), 111.28 (s), 69.29 (s), 35.73 (s), 33.56 (s), 32.58 (s), 24.61 (s), 20.55 (s), 17.69 (s), 17.54 (s). HRESIMS $[\text{M}+\text{H}]^+ m/z$ 491.1904 (Calcd for $\text{C}_{28}\text{H}_{29}\text{NO}_7$ 491.1944).

(R)-1-(5,8-dihydroxy-1,4-dioxo-1,4-dihydronaphthalen-2-yl)-4-methylpent-3-en-1-yl 5-(diphenylamino)-5-oxopentanoate (M16)

Red oil, yield 53%. ^1H NMR (600 MHz, CDCl_3) δ 12.58 (s, 1H), 12.42 (d, $J = 4.8$ Hz, 1H), 7.49–7.41 (m, 2H), 7.40–7.33 (m, 5H), 7.21–7.16 (m, 3H), 7.08 (d, $J = 7.8$ Hz, 1H), 6.93 (d, $J = 10.9$ Hz, 2H), 6.04–5.93 (m, 1H), 5.07 (t, $J = 7.2$ Hz, 1H), 2.86–2.76 (m, 2H), 2.46 (dt, $J = 15.9, 7.4$ Hz, 3H), 2.34 (dt, $J = 27.7, 7.0$ Hz, 3H), 1.66 (s, 3H), 1.55 (s, 3H). ^{13}C NMR (151 MHz, CDCl_3) δ 178.20 (s), 176.73 (s), 173.21 (s), 172.30 (s), 167.39 (s), 166.86 (s), 148.21 (s), 142.70 (s), 142.62 (s), 136.10 (s), 132.86 (s), 132.67 (s), 131.48 (s), 129.79 (s), 128.97 (s), 126.43 (s), 117.62 (s), 111.79 (s), 111.55 (s), 69.29 (s), 34.06 (s), 33.34 (s), 32.83 (s), 25.77 (s), 20.72 (s), 17.95 (s). HRESIMS $[\text{M}+\text{H}]^+ m/z$ 553.2081 (Calcd for $\text{C}_{33}\text{H}_{31}\text{NO}_7$ 553.2101).

4.4. Cell lines and culture conditions

The cell lines used in our work were human breast cancer cell lines (MCF-7, MDA-MB-231), human cervical cancer cell line (HeLa), human colon cancer cell line (HCT-8), human lung adenocarcinoma cell line (A549), and human normal breast epithelial cell line (MCF-10A). All cell lines were obtained from the State Key Laboratory of Pharmaceutical Biotechnology, Nanjing University. Amongst, MCF-7, MDA-MB-231, HeLa and A549 cell lines were cultured in DMEM/high glucose supplemented with 10% fetal bovine serum and 1% penicillin/streptomycin. HCT-8 cell line was maintained in RPMI medium 1640 basic supplemented with 10% fetal bovine serum and 1% penicillin/streptomycin. MCF-10A cell line was maintained in MEpiCM. All cells were incubated at 37 °C in a humidified atmosphere containing 5% CO_2 .

4.5. cck-8 assay

The anti-proliferation assay was performed by using CCK-8 assay. Cells were cultured in medium to log phase and then digested, centrifuged and resuspended in fresh medium. Then, they were seeded into 96 well plates (10^4 cells / well) and incubated overnight at 37 °C in 5% CO_2 to make them reattach. Subsequently, cells were treated by the target compounds at increasing concentrations (0.1, 1, 10 and 100 μM) for another 24 h. Then, the cell viability was detected in CCK-8 assay and operated in strict accordance with the manufacturer instructions. Using ELISA reader (EPOCH, BioTek, USA) to read the absorbance (OD_{450}). The positive drug was PTX [30]. There are three repeated wells for each

concentration, and each experiment was repeated three times. The IC_{50} value was defined as a concentration that caused 50% loss of cell viability, which was calculated by Origin 7.5.

4.6. Cell cycle analysis

Targeted cells (MDA-MB-231) cells were seeded in 6-well plates (5.0×10^4 cells/well) and incubated at 37 °C in the 5% CO_2 incubator for 12 h. Then, the exponential cells were exposed to different concentrations of M9 (0, 1, 2, 4 μM) and 4 μM SK for 24 h. For the time-dependent assay, the adherent cells were pre-treated with 2 μM M9 and SK for 0, 24, 36, and 48 h. The cells were centrifuged with (2000 rpm, 4 °C, 10 min) and fixed in 70% cooled ethanol at –20 °C for overnight. Whereafter, cells were re-suspended in binding buffer containing 0.1 mg/mL RNase A and 5 $\mu\text{g}/\text{mL}$ propidium iodide (PI). Flow cytometry (BD FACS Calibur, USA) was used to determine the DNA content of cells for cell cycle distribution analysis, at least 10,000 events were plotted for each sample. The cell percentages of G0/G1, S and G2/M phases was measured by Flowjo7.6 software.

4.7. Flow cytometric analysis of apoptosis

Cell apoptosis was measured by using Annexin V-FITC/PI double staining. Briefly, MDA-MB-231 cells were seeded in 6-well plates with 5.0×10^3 cells /well, cultured overnight at 37 °C in 5% CO_2 incubator, and then treated with M9 (0, 1, 2, 4 μM) and 4 μM SK for 24 h in the dose-dependent test. Cells were harvested and washed twice with PBS and then stained with Annexin V-FITC (5 μL) and PI (5 μL) in the binding buffer for 15–20 min at room temperature away from light. Finally, using BD Accuri C6 Flowjo Cytometer (BD, USA) to measure the apoptotic cells. Data analysis was performed by using Flowjo 7.6 software. The percentage of cells distributed in the right quadrant (Annexin V +) was used for statistics analysis using Graphpad prism 8.

4.8. Wound-healing assay

MDA-MB-231 cells were seeded in 6-well culture plates with 2×10^5 cells/ cm^2 and were cultured overnight. When the cell density is above 90%, the monolayer cells were scraped using microtubule tips to form scratches. Next, cells were washed with PBS three times, and incubated in serum-free medium with different concentrations of M9, SK and PTX. The wound healing was observed with microscopy (NIKON, Japan), and the scratches were photographed at 0, 24 and 48 h. Then, NIH Image J image analysis software was used to delineate the wound areas for analysis.

4.9. Trans-well assay

MDA-MB-231 cells were pretreated with M9, SK and PTX for 24 h and were then seeded in serum-free media on the upper side of a trans-well plate. Next, cells were allowed to migrate towards media containing 10% of FBS (in the lower side) for 24 h. After the incubation period, cells on the lower side of the membrane were fixed with methanol for 10 min and were then stained with 1% crystal violet for 5 min. After that, cells were washed with PBS for 3 to 5 times. Finally, the stained cells were observed under microscope (five random fields at $\times 100$ magnification).

4.10. Colony formation assay

MDA-MB-231 cells were treated with M9, SK and PTX for 24 h. Cells were then collected and diluted into 1×10^2 cells/mL cell suspension with complete medium. 1 mL of cell suspension was added into each well of 12 well plate, and then grew at 37 °C in 5% CO_2 atmosphere for 7 days. The medium was replaced every 2–3 days. The culture was terminated until obvious clones appeared in the dish. Washing the clones thrice with PBS and fixed them with 4% paraformaldehyde for

15–20 min. After that, staining the clones with 1% crystal violet dye for 30 min and then washing them for 3 to 5 times with PBS. Finally, the 12-well plate was placed upside down to drain the PBS. The cells were observed under a microscope. Each experiment was repeated at least three times.

4.11. Western blot analysis

MDA-MB-231 cells were lysed with RIPA lysis buffer containing 1% protease and phosphatase inhibitor cocktail I (Target Mol, USA) to extract the total proteins. Then, using BCA protein assay kit to determine protein concentration. About 60 µg of total protein was separated by 10% SDS-polyacrylamide gels and then transferred to PVDF membrane. Membranes were then sealed with 5% skim milk solution for 1 h and were incubated with diluted primary antibody (1:1000 dilution) at 4 °C and shaken gently overnight. After washing with TBST for 30 min (change TBST every 5 min), membranes were incubated with secondary antibodies (1:5000–1:10000 dilution) for another 1 h at room temperature. Bands were developed by super ECL detection reagent and photographed by Tanon 5200 digital camera (Tanon, China). Finally, Image J software (National Institutes of Health, Bethesda, Maryland, USA) was used to analyze the results, and all target proteins were standardized by reference to GAPDH.

4.12. Docking simulation

The crystal structures of protein complexes were retrieved from the RCSB protein database. Compound molecules bind to Akt (PDB Code: 3cqw) by DS-CDOCKER, a graphical user interface in Discovery Studio 3.5. All binding water and ligands were removed from the protein. After molecular docking, the interaction types between the ligand-based pharmacophore model and the docking protein were analyzed.

4.13. 3D-QSAR

3D-QSAR is a reliable method to better understand the SAR spectra of synthetic compounds. All compounds were divided into two parts: training set and test set. The anti-proliferative activity of the compounds was used for QSAR analysis. The reliability of QSAR model could be evaluated by cross-validation correlation coefficient.

Declaration of Competing Interest

The authors declare that they have no known competing financial interests or personal relationships that could have appeared to influence the work reported in this paper.

Acknowledgements

This research was supported by the National Natural Science Foundation of China (NSFC) (U1903201, 21702100, 21907051), the Program for Changjiang Scholars and Innovative Research Team in University (IRT_14R27), and the Natural Science Foundation of Jiangsu Bureau of Science and Technology (BK20191254), and the Fundamental Research Funds for the Central Universities (020814380140, 020814380151).

Appendix A. Supplementary material

Supplementary data to this article can be found online at <https://doi.org/10.1016/j.bioorg.2021.104872>.

References

- [1] S.M. Albeshan, M.G. Mackey, S.Z. Hossain, A.A. Alfuraih, P.C. Brennan, Breast cancer epidemiology in gulf cooperation council countries: a regional and international comparison, *Clin. Breast Cancer* 18 (3) (2018) E381–E392.
- [2] F. Bray, J. Ferlay, I. Soerjomataram, R.L. Siegel, L.A. Torre, A. Jemal, Global cancer statistics 2018: GLOBOCAN estimates of incidence and mortality worldwide for 36 cancers in 185 countries, *CA Cancer J. Clin.* 68 (6) (2018) 394–424.
- [3] B.D. Lehmann, J.A. Bauer, X. Chen, M.E. Sanders, A.B. Chakravarthy, Y. Shyr, J. A. Pietenpol, Identification of human triple-negative breast cancer subtypes and preclinical models for selection of targeted therapies, *J. Clin. Invest.* 121 (7) (2011) 2750–2767.
- [4] W.D. Foulkes, I.E. Smith, J.S. Reis, Triple-negative breast cancer, *New Engl. J. Med.* 363 (20) (2010) 1938–1948.
- [5] E.A. Rakha, M.E. El-Sayed, A.R. Green, A.H.S. Lee, J.F. Robertson, I.O. Ellis, Prognostic markers in triple-negative breast cancer, *Cancer* 109 (1) (2007) 25–32.
- [6] K. Gelmon, R. Dent, J.R. Mackey, K. Laing, D. McLeod, S. Verma, Targeting triple-negative breast cancer: optimising therapeutic outcomes, *Ann. Oncol.* 23 (9) (2012) 2223–2234.
- [7] P.F. McAuliffe, F. Meric-Bernstam, G.B. Mills, A.M. Gonzalez-Angulo, Deciphering the role of PI3K/Akt/mTOR pathway in breast cancer biology and pathogenesis, *Clin. Breast Cancer* 10 (2010) S59–S65.
- [8] X.Y. Zhang, Y. Liu, Y.P. Jia, Q. Zhao, W.Y. Wang, Z. Zhang, W. Li, L.C. Sun, Ameliorative effect of acetylshikonin on cigarette smoke induced lung inflammation in mice, *Lat. Am. J. Pharm.* 38 (9) (2019) 1862–1873.
- [9] X. Chen, L. Yang, N. Zhang, J.A. Turpin, R.W. Buckheit, C. Osterling, J. J. Oppenheim, O.M.Z. Howard, Shikonin, a component of Chinese herbal medicine, inhibits chemokine receptor function and suppresses human immunodeficiency virus type 1, *Antimicrob. Agents Ch.* 47 (9) (2003) 2810–2816.
- [10] X.Y. Huang, H.L. Fu, H.Q. Tang, Z.Q. Yin, W. Zhang, G. Shu, L.Z. Yin, L. Zhao, X. R. Yan, J.C. Lin, Optimization extraction of Shikonin using ultrasound-assisted response surface methodology and antibacterial studies, *Evid-Based Compl. Alt.* 2020 (2020) 1–10.
- [11] N. Guo, R. Miao, X. Gao, D. Huang, Z. Hu, N. Ji, Y. Nan, F. Jiang, X. Gou, Shikonin inhibits proliferation and induces apoptosis in glioma cells via downregulation of CD147, *Mol. Med. Rep.* 19 (5) (2019) 4335–4343.
- [12] J.C. Boulos, M. Rahama, M.F. Hegazy, T. Efferth, Shikonin derivatives for cancer prevention and therapy, *Cancer Lett.* 459 (2019) 248–267.
- [13] B. Wiench, Y.R. Chen, M. Paulsen, R. Hamm, S. Schroder, N.S. Yang, T. Efferth, Integration of different “-omics” technologies identifies inhibition of the IGF1R-Akt-mTOR signaling cascade involved in the cytotoxic effect of Shikonin against Leukemia cells, *Evid-Based Compl. Alt.* (2013) 1–11.
- [14] F. Ni, X.B. Huang, Z.Z. Chen, W.B. Qian, X.M. Tong, Shikonin exerts antitumor activity in Burkitt’s lymphoma by inhibiting C-MYC and PI3K/AKT/mTOR pathway and acts synergistically with doxorubicin, *Sci. Rep.-Uk* 8 (1) (2018) 3317.
- [15] B.Y. Li, Z.G. Yuan, J. Jiang, Y.Q. Rao, Anti-tumor activity of Shikonin against afatinib resistant non-small cell lung cancer via negative regulation of PI3K/Akt signaling pathway, *Biosci. Rep.* 38 (6) (2018).
- [16] Y. Chen, T.T. Wang, J. Du, Y.C. Li, X. Wang, Y. Zhou, X.X. Yu, W.M. Fan, Q.J. Zhu, X.M. Tong, Y. Wang, The critical role of PTEN/PI3K/AKT signaling pathway in Shikonin-induced apoptosis and proliferation inhibition of chronic myeloid leukemia, *Cell. Physiol. Biochem.* 47 (3) (2018) 981–993.
- [17] Y.Z. Zhu, Y. Zhong, X. Long, Z. Zhu, Y. Zhou, H. Ye, X.B. Zeng, X.B. Zheng, Deoxyshikonin isolated from *Arnebia euchroma* inhibits colorectal cancer by down-regulating the PI3K/Akt/mTOR pathway, *Pharm. Biol.* 57 (1) (2019) 412–423.
- [18] S. Jiang, H.T. Wang, Y. Guo, Z. Liu, W. Song, Acetylshikonin inhibits the migration and invasion of A375 cells by reversing EMT process via the PI3K/Akt/mTOR pathway, *Biotechnol. Biotech. Eq.* 33 (1) (2019) 699–706.
- [19] R. Deng, J. Tang, B.F. Xie, G.K. Feng, Y.H. Huang, Z.C. Liu, X.F. Zhu, SYUNZ-16, a newly synthesized alkannin derivative, induces tumor cells apoptosis and suppresses tumor growth through inhibition of PKB/AKT kinase activity and blockade of AKT/FOXO signal pathway, *Int. J. Cancer* 127 (1) (2010) 220–229.
- [20] Y.Y. Yang, H.Q. He, J.H. Cui, Y.J. Nie, Y.X. Wu, R. Wang, G. Wang, J.N. Zheng, R. D. Ye, Q. Wu, S.S. Li, F. Qian, Shikonin derivative DMAKO-05 inhibits akt signal activation and melanoma proliferation, *Chem. Biol. Drug Des.* 87 (6) (2016) 895–904.
- [21] A. Eng, V. McCormack, I.d.-S.-S.J.P. medicine, Receptor-defined subtypes of breast cancer in indigenous populations in africa: a systematic review and meta-analysis, *PLOS Med.* 11 (9) (2014).
- [22] B. Roy, A.K. Pattanaik, J. Das, S.K. Bhutia, B. Behera, P. Singh, T.K. Maiti, Role of PI3K/Akt/mTOR and MEK/ERK pathway in Concanavalin A induced autophagy in HeLa cells, *Chem. Biol. Interact.* 210 (2014) 96–102.
- [23] S. Kumar, S.K. Guru, A.S. Pathania, S. Manda, A. Kumar, S.B. Bharate, R. A. Vishwakarma, F. Malik, S. Bhushan, Fascaplysin induces caspase mediated crosstalk between apoptosis and autophagy through the inhibition of PI3K/AKT/mTOR signaling cascade in human leukemia HL-60 cells, *J. Cell. Biochem.* 116 (6) (2015) 985–997.
- [24] S. Ebrahimi, M. Hosseini, S. Shahidsales, M. Maftouh, G.A. Ferns, M. Ghayour-Mobarhan, S.M. Hassanian, A. Avan, Targeting the Akt/PI3K signaling pathway as a potential therapeutic strategy for the treatment of pancreatic cancer, *Curr. Med. Chem.* 24 (13) (2017) 1321–1331.
- [25] X. Cheng, J.B. Shi, H. Liu, L.Z. Chen, Y. Wang, W.J. Tang, X.H. Liu, Discovery of (4-bromophenyl)(3-hydroxy-4-methoxyphenyl) methanone through upregulating hTERT induces cell apoptosis and ERS, *Cell Death Dis.* 8 (2017) e3016.
- [26] Y. Ke, J.J. Liang, R.J. Hou, M.M. Li, L.F. Zhao, W. Wang, Y. Liu, H. Xie, R.H. Yang, T.X. Hu, J.Y. Wang, H.M. Liu, Synthesis and biological evaluation of novel Jiyuan Oridonin A-1,2,3-triazole-azole derivatives as antiproliferative agents, *Eur. J. Med. Chem.* 157 (2018) 1249–1263.

- [27] H.Y. Lin, H.W. Han, W.X. Sun, Y.S. Yang, C.Y. Tang, G.H. Lu, J.L. Qi, X.M. Wang, Y. H. Yang, Design and characterization of alpha-lipoic acyl shikonin ester twin drugs as tubulin and PDK1 dual inhibitors, *Eur. J. Med. Chem.* 144 (2018) 137–150.
- [28] W.X. Sun, H.W. Han, M.K. Yang, Z.L. Wen, Y.S. Wang, J.Y. Fu, Y.T. Lu, M.Y. Wang, J.X. Bao, G.H. Lu, J.L. Qi, X.M. Wang, H.Y. Lin, Y.H. Yang, Design, synthesis and biological evaluation of benzoylacrylic acid shikonin ester derivatives as irreversible dual inhibitors of tubulin and EGFR, *Bioorg. Med. Chem.* 27 (23) (2019) 115153.
- [29] S. Fattahi, F. Amjadi-Moheb, R. Tabaripour, G.H. Ashrafi, H. Akhavan-Niaki, PI3K/AKT/mTOR signaling in gastric cancer: epigenetics and beyond, *Life Sci.* 262 (2020) 118513.
- [30] P. Chowdhury, P.K.B. Nagesh, E. Hatami, S. Wagh, N. Dan, M.K. Tripathi, S. Khan, B.B. Hafeez, B. Meibohm, S.C. Chauhan, M. Jaggi, M.M. Yallapu, Tannic acid-inspired paclitaxel nanoparticles for enhanced anticancer effects in breast cancer cells, *J. Colloid Interface Sci.* 535 (2019) 133–148.